THE SOCIETY OF NAVAL ARCHITECTS AND MARINE ENGINEERS
and
THE SHIP STRUCTURE COMMITTEE

Paper presented at the Ship Structures Symposium '93
Sheraton National Hotel, Arlington, Virginia, November 16-17, 1993

A Finite Element Assessment of the Buckling Strength Equations of Stiffened Plates

S. Z. Hu[1]

[1]Defence Research Establishment Atlantic, Dartmouth, Nova Scotia, Canada

Abstract

The collapse of in-plane loaded stiffeners in ship structures causes simultaneous buckling of adjacent plates. DMEM10 (Structural Design of Surface Warship, Canadian Forces) and NES110 (Naval Engineering Standard, UK MOD) evaluate the ultimate strength of a stiffened plate in a way that the ultimate load carrying capacity is obtained by iterating between the ultimate plate compressive strength curve and the column strength curve. Currently, the ultimate compressive plate strength is obtained based on Faulkner's effective width equation, while the combined stiffener and plate strength is evaluated by Bleich's parabola. The original derivation of the parabolic curve only takes the material inelasticity into account without considering imperfections. Smith et al. have derived sets of column strength curves for small, average and large imperfections based on finite element results. These results are presented in a data sheet format in SSCP23 (Design of Surface Ship Structures, UK MOD). A comparison between the ultimate strength of the conventional procedure and the design curves in SSCP23 shows substantial discrepancies. Finite element analyses, including the effects of imperfections and residual stresses, are employed to study these discrepancies. In order to provide alternatives in design procedures, some related provisions in civil structural and offshore construction standards are also examined.

Introduction

Steel plates used in ship and offshore structures are reinforced by stiffeners in orthogonal directions. Fabrication of such stiffened plates requires plates to be fully welded to stiffeners. The fabrication process generates geometric imperfections and residual stresses in both plates and stiffeners which significantly affect the buckling strength of the stiffened plates, especially in the elastic-plastic region. In addition, the collapse of the stiffener causes simultaneous buckling of adjacent plates. Thus, the evaluation of ultimate strength and prediction of the load-displacement history is difficult.

This paper starts with a review of the design equations and procedures for stiffened plates under in-plane loading in current Canadian and British ship design standards; namely DMEM10 [1], NES110 [2] and SSCP23 [3]. Some provisions related to the buckling strength of stiffened plates in civil structural steel and offshore construction standards such as S136 [4] and S473 [5] are also examined.

Nonlinear finite element analyses of unstiffened and stiffened plates including geometric and material non-linearities were performed using the commercial finite element program ADINA [6]. The effects of initial imperfections and residual stresses of the plate were included in the finite element models by using the procedure proposed by the author [7, 8] to verify the code equations.

Design Procedures in Different Standards

The buckling of stiffened plates involves two basic components, the plates and the stiffeners. The plate may buckle between stiffeners before the failure of the stiffener. The stiffener may buckle and cause the adjacent plates to deform, producing a column-like buckling failure. Because the buckling stress of the stiffened plate is a function of the slenderness ratio, and because the 'effective' width of the plate at the time of the buckling is a function of the applied stress, the evaluation of the buckling stress of the stiffened plate in most standards uses a column strength formula and an effective plate width equation.

The effective width concept is frequently used in the design of thin-walled metal structures and has been applied to metal ship structural design for some time in order to account for the post-buckling reduction of strength. After the occurrence of local plate buckling between stiffeners, a portion of the pre-buckling load on the centre

strip of the plate is transferred to the edges. As a result, a non-uniform stress distribution is developed. The concept assumes that the redistribution of stress continues until the stress at the edges reaches the yield stress of the material and the plate begins to fail. At the time of failure, the load is entirely taken by the yielding strips of the plate adjacent to the supported edges, while the central portion takes no load. Numerous test results show that the effective width is a function of material properties, boundary conditions, residual stress level and loading conditions. This concept may work well for plate failure alone. When this concept is applied to stiffened plates, the failure modes are more complicated. The stiffened plate may fail before the plate can reach its maximum carrying capacity or may not fail until plates enter the descending branch in their load displacement curve.

The buckling stress of members is usually expressed in terms of a slenderness ratio which is defined by the geometric and material properties of the member. For a stiffened plate of length *l*, width b and thickness t, one slenderness ratio describes the plate, while another describes the combination of stiffener and plate. Because of different definitions in different standards, we may define two plate slenderness parameters β and β_y as

$$\beta = \frac{b}{t}\sqrt{\frac{\sigma_c}{E}}; \quad \beta_y = \frac{b}{t}\sqrt{\frac{\sigma_y}{E}}$$

where σ_c is the plate buckling stress, σ_y is the yield stress and E is the Young's modulus. On the other hand, two non-dimensional column slenderness ratios may be defined as

$$\lambda = \frac{L}{\pi r}\sqrt{\frac{\sigma_y}{E}}; \quad \lambda_e = \frac{l}{\pi r_e}\sqrt{\frac{\sigma_y}{E}}$$

where r and r_e are the radius of gyration for a plate with full width and effective width, respectively.

DMEM10 and NES110 use Faulkner's [9, 10, 11] equation which defines the effective width ratio as

$$\frac{b_e}{b} = 1 - \frac{2\eta}{b/t - 2\eta}\left(\frac{3.62\beta^2}{13.1 + 0.25\beta^4}\right)^2; \quad 0<\beta\le 1$$
$$= \frac{2}{\beta} - \frac{1}{\beta^2} - \frac{2\eta}{b/t - 2\eta}\left(\frac{3.62\beta^2}{13.1 + 0.25\beta^4}\right)^2; \quad 1<\beta\le 2.69$$
$$= \frac{2}{\beta} - \frac{1}{\beta^2} - \frac{2\eta}{b/t - 2\eta}; \quad 2.69<\beta$$

where η is a parameter which defines the level of the residual stresses. The last term in this equation takes into account the strength reduction due to the residual stress effect. The residual stress pattern in this equation is ideally set as rectangular tensile and compressive stress blocks with the width of the tensile stress block set as ηt. It is usually assumed that $\eta = 3$ for ship design after shakedown. The curves in DMEM10 and NES110 are obtained by a further assumption that $E^2/\sigma_y^2 = 900$ which implies that $b/t = 30\beta$ for a typical welded ship. For the overall buckling of the stiffened plate, they use the CRC parabolic column strength curve [12] which is based on Bleich's derivation [13] as

$$\frac{\sigma_c}{\sigma_y} = 1.0 - 0.25\lambda_e^2; \quad 0<\lambda_e<\sqrt{2}$$
$$\frac{\sigma_c}{\sigma_y} = \lambda_e^{-2}; \quad \sqrt{2}\le\lambda_c$$

Although this equation was originally derived to take into account the residual stress effect, it has also been used widely to account for other strength reduction factors. In addition to flexural buckling, it has been used in various structural design standards for members in torsional buckling and lateral torsional buckling design. The radius of gyration 'r' in the parabolic column strength curve is calculated using the effective plating which is a function of the applied stress. An iterative procedure is used between Faulkner's effective width equation and the parabolic column curve. With an initial estimate of the buckling stress, one can obtain the effective width and the effective radius of gyration. Subsequently, one can compare the buckling stress with the initial estimate until the solution converges.

The S136 manual uses Winter's test results [14] for the effective width as

$$\frac{b_e}{b} = \frac{1.9}{\beta} - \frac{0.79}{\beta^2}; \quad \beta>1.287$$
$$\frac{b_e}{b} = 1; \quad \beta\le 1.287$$

and uses the parabolic column strength curve for the stiffened plate buckling as

$$\frac{\sigma_c}{\sigma_y} = 1.0 - 0.25\lambda^2; \quad 0<\lambda<\sqrt{2}$$
$$\frac{\sigma_c}{\sigma_y} = \lambda^{-2}; \quad \sqrt{2}\le\lambda$$

Although the plate slenderness ratio parameter is a function of the instantaneous buckling stress, the radius of gyration r in the parabolic column curve is calculated using the full plate width. Therefore, there is no need for an iterative procedure. The compressive buckling strength of the stiffened plate can be obtained by multiplying the buckling stress with the effective area.

S473 defines the effective width ratio as

$$\frac{b_e}{b}=\left(\frac{1.8}{\beta_y}-\frac{0.8}{\beta_y^2}\right)\times c_y\times c_{xy}\;;\quad b_e\le b$$

where c_y and c_{xy} account for further reduction due to transverse compressive stress and shear stresses, respectively. The overall column buckling stress is obtained by using multi-column curves proposed by SSRC [11]. Three sets of curves are published in terms of the non-dimensional slenderness ratio based on Lehigh University's research of 112 computed maximum strength curves. Curve 2 is listed as follows:

$$\sigma_c/\sigma_y = 1; \qquad 0\le\lambda_e\le 0.15$$
$$\sigma_c/\sigma_y = 1.035 - 0.202\lambda_e - 0.222\lambda_e^2; \qquad 0.15<\lambda_e\le 1.0$$
$$\sigma_c/\sigma_y = -0.111 + 0.636\lambda_e^{-1} + 0.087\lambda_e^{-2}; \qquad 1.0<\lambda_e\le 2.0$$
$$\sigma_c/\sigma_y = 0.009 + 0.877\lambda_e^{-2}; \qquad 2<\lambda_e\le 3.6$$
$$\sigma_c/\sigma_y = \lambda_e^{-2}; \qquad 3.6<\lambda_e$$

The plate slenderness ratio parameter in S473's effective width equation is a function of the yield stress of the material. After obtaining the effective width, the effective radius of gyration can be obtained. The compressive buckling strength can be calculated by multiplying the buckling stress in the SSRC multi-column strength curves with the effective area.

Smith et al. [15] presented a set of data sheets in graphic format to evaluate the average buckling stresses of the stiffened plates. With various assumed imperfections and the application of nonlinear finite element programs, they produced sets of column curves representing small, average and large imperfections and validated them with experimental results. Because these curves are plotted in term of stress ratio versus stiffened plate slenderness ratio with full plate width and for various plate slenderness ratio parameters, there is no need of iteration. In these curves it is assumed that the ratio of the cross sectional areas of the stiffener 'A_s' to the plate 'A' equals 0.2. SSRC23 currently adopts these curves as data sheets. In fact, the buckling stress in DMEM10 and S473 also can be evaluated and expressed in term of stress ratio versus stiffened plate slenderness ratio parameter with full plate width. The comparison of the column strength curves of SSCP23 with average imperfections, DMEM10 withη = 3 and S473 with the SSRC curve 2 are shown in Figure 1. Substantial discrepancies between various standards exist.

Finite Element Analysis

The finite element study was performed with the commercial software ADINA which enabled modelling of elastic-plastic material properties and large deformations.

A four-node quadrilateral shell, from the family of the degenerate iso-parametric shell elements, with a $2\times2\times2$ integration order was used to model the plate and stiffener. The kinematic assumption was large displacement and rotation but small strain. The material modelling of the plate is assumed to be bilinear elastic-perfectly-plastic with a von Mises yield condition. Both a load-displacement control method and an automatic-displacement control method were used in the solution scheme.

The imperfections were generated either through extraction of the first linear buckling mode or with static deformed geometry. Therefore, linear buckling analysis or linear static analysis with distributed loads or prescribed displacements were performed before the incremental load-displacement analysis.

Both unstiffened and stiffened plates with the plate slenderness parameter ratio β equal to 1,2,3 or 4 were analyzed. The aspect ratio *l*/b of the plate was 1.5. The stiffener in the stiffened plate was assumed to have a cross section approximating a standard type no. 6 'T' bar. The area of the stiffener A_s was approximately 20 percent of the area of the plate $b\times t$ in all the stiffened plates. The non-dimensional slenderness ratio λ of the stiffened plate calculated with a full plate width was 0.3 or 0.6. A summary of the dimensions for the plates and stiffened plates is given in Tables 1 and 2, respectively. The boundary condition of the plate was assumed to be simply-supported along four edges while the boundary condition of the stiffened plate was assumed to be simply-supported at the ends with symmetry along the longitudinal edges. Because of the assumed symmetric geometry of the plates and stiffeners, only one-quarter of the plate and the stiffened plate are modelled.

One of the focus points in this investigation is the initial geometric imperfections. Two sets of imperfections should be defined. One is the distorted profile in the plate, the other the out-of-straightness in the stiffener as shown in Figure 2. Smith et al. [14] have reported that the imperfections in a plate can be assumed to be proportional to β^2. They suggest that the initial deformation w_o for the average imperfection is $0.1\beta^2 t$. The maximum permissible camber tolerance w_s for a standard shape is usually assumed to be 0.2% of the length [15]. Different imperfections are examined and will be explained later.

The other focal point of the investigation is the magnitude and distribution of residual stresses in the stiffened plate. One of the common assumptions is that the residual stress pattern is in rectangular tensile and compressive stress blocks in the transverse direction and constant in the longitudinal direction. However, the residual stress in a real plate is in a tri-axial state and varies not only in the transverse direction but also parallel to the weld as shown in Figure 3. It was decided to introduce the residual stress in the plate in a way that resembles the actual welding procedure. The residual stresses thus were generated

through temperature variations on nodal points adjacent to the weld. The magnitude of the residual stress can be calibrated by changing the temperature value.

The introduction of thermal residual stress causes deformation of the model and changes nodal coordinates that are inconsistent with the input geometric imperfections, since the geometry after welding (after introducing residual stress) should be used as the initial geometry. To avoid the change of the initial imperfection, a procedure developed by the author [6, 7] is used. This procedure has been successfully applied and verified in fabricated tubular structures used in offshore oil platforms. Figure 4 shows the procedure used for the automatic generation of welding residual stresses with retention of initial imperfection and is explained as follows:

Step 1. Create imperfections through buckling analysis or static analysis and generate the finite element mesh while the nodes adjacent to the weld have positive temperature loading.

Step 2. Activate temperature loading and produce reversed residual stresses. The plate is strained in the opposite sense to the final residual stress distribution. The updated nodal geometry is stored in a file.

Step 3. Read this geometry file as the original geometry; therefore the imperfections in the model include geometric imperfections and displacements due to positive temperature variations. The plate is free of residual stresses. The nodes adjacent to the weld have negative temperature loading.

Step 4. Activate the temperature loading at the first loading step. This results in a plate with the desired residual stresses and imperfections approximating the initial imperfections. The imperfections can be verified by comparing the nodal coordinates of the plate at the end of this step with step 1. The plate, therefore, will have desired imperfections and residual stresses.

Numerical Results

Models with residual stresses have been verified by comparing the nodal geometry in step 4 with that in step 1. The differences in nodal geometry are negligible. In some cases, models with nodal geometry in step 4 with residual stress removed are re-run and compared with the results from models with the nodal geometry in step 1. The results show that there are no differences in load-displacement response. Therefore, the approximation of the imperfections at step 4 can be regarded as the original input imperfections.

After negative nodal temperature changes, a residual stress pattern with tensile stress close to the yield stress of the material is created. The average stresses in the integration points in a direction parallel to the weld for two different plate slenderness ratio parameters are plotted in Figure 5 along with Faulkner's residual stress patterns. The terms 'edge' and 'centre' in this figure refer to the nearest integration points to the edge and centre, respectively. The finite element results show that the residual stress is not only varied along the transverse direction but also in the longitudinal direction. The stresses are higher in the centre portion of the plate and gradually decrease to zero at the edges (there is no applied stress at the edges) while Faulkner's stress pattern gives uniform magnitude along the longitudinal direction.

The comparison of the load-shortening curves shows that the residual stresses decrease the average buckling stresses for plates as shown in Figure 6 (a). It also shows that the residual stresses decrease the average buckling stresses of stiffened plates for different slenderness ratios as shown in Figure 6 (b) and (c). Stiffened plates with the same plate slenderness parameters but different slenderness ratios show that the larger the slenderness ratio, the smaller the buckling stress as shown in Figure 6 (d). In addition, the slope of the descending branch of the load-displacement curves for longer plates is steeper, especially for plates with bigger plate slenderness parameters.

The reduction of the buckling stresses depends on the level of the residual stresses. The load-displacement curves of two stiffened plates with different levels of residual stresses are shown in Figure 7. It is interesting to see that the residual stress not only causes the load-displacement curve to turn into the plastic region earlier but also shifts the load-displacement curve for the thicker plate. The strength reduction effects, however, depend on the plate slenderness parameters which, in turn, decide the load-displacement characteristics.

The maximum stress ratios (σ/σ_y) for plates with different β are summarized in Table 1, while the stress ratios (σ/σ_y) for stiffened plates with different β and imperfections are summarized in Table 2. The comparison of the stress ratios with the results of DMEM10 and SSCP23 are also listed in Table 2 and graphically presented in Figure 8. The results show that the imperfections decrease the buckling stresses significantly without exception. For example, the buckling stress ratios of a stiffened plate with $\lambda = 0.6$ and $\beta = 2$ reduce from 0.84 to 0.53 (37 % decrease) as the imperfections increase from $0.0002l$ to $0.01l$. The residual stresses also decrease the buckling stress ratios depending on the value of β. The buckling

stress ratio may decrease 2.2 % for a short, thick plate and 7.2 % for a long, thin plate. The comparison of the results with standards shows that the current iteration procedure gives higher strength than the finite element predictions. The comparison in Figure 8 also shows very good correlation between the finite element results and the results of SSCP23.

β	t(mm)	(1)	(2)
1	38.25	1.00	0.98
2	19.125	0.82	0.74
3	12.75	0.56	0.51
4	9.56	0.45	0.42

material: E=205,000 MPa, σ_y=300 MPa, α=11.7x10 $^{-6}$/°C
geometry: b = 1000 mm, l = 1500 mm
(1) no residual stresses
(2) with 200°C temperature variation

Table 1
Summary of the Geometry and the Maximum Stress Ratio (σ/σ_y) of the Plates

Conclusion

It has been shown that imperfections in plates and stiffeners can have a significant effect on the buckling strength of stiffened plates. The fabrication tolerance such as the maximum allowable imperfections in plates, sweeps and cambers (out-of-straightness in minor and major axes) in stiffeners should be clearly defined.

This paper has discussed four different design procedures of stiffened plates in ship structural, civil structural and offshore constructional standards. The four different procedures can result in substantial discrepancies in buckling strength of the stiffened plates. The variations in the equations and procedures may be caused by the systematic differences in the test set-up, the fabrication technique, the collected data and the interpretation of the results amoung various establishments. There is no intention here to comment on whether one procedure is superior to the others. But it is clear that the procedure should be easy to use, be able to give engineers an intuitive understanding of the design equations and be able to cover all possible cases including different dimensions, boundaries and loadings.

The method that was used to introduce residual stresses into the finite element model, without causing unwanted distortions, proved to be very successful in modelling stiffened plates. The method of applying initial stress is very complicated because of the tri-axial variation and the self-equilibrium of the residual stresses. The unbalanced moment at any cross section will result in additional deformation of the plate. The use of nodal temperature change in the weld regions to simulate the weld-introduced residual stresses is the most natural way, with little effort, and the self-equilibrium of the initial stress is guaranteed.

Qualitative comparison has shown the finite element results have the same tendency as those given by the current design procedures. Quantitative comparison, however, indicates that the design procedures may over-estimate the buckling strength of stiffened plates. The over-estimate, however, may be compensated by a larger safety factor or by overestimated loading in current standards. There are

λ	l(mm)	b(mm)	t(mm)	β	(1)	(2)	(3)	(4)	(5)	(6)	SSCP23	DMEM10
0.3	1720	570	21.9	1	0.77				0.91	0.89	0.87	0.96
	1720	810	15.4	2	0.66	0.78			0.73	0.68	0.70	0.73
	1720	990	12.6	3	0.52		0.81	0.90	0.56	0.52	0.54	0.57
	1740	1140	10.9	4	0.45				0.47	0.44	0.45	0.50
0.6	3500	570	21.9	1	0.55	0.74			0.86	0.82	0.85	0.90
	3420	810	15.4	2	0.53	0.71	0.77	0.84	0.71	0.67	0.68	0.69
	3420	990	12.6	3	0.48		0.56	0.58	0.55	0.51	0.53	0.54
	3420	1140	10.9	4	0.43				0.46	0.43	0.44	0.46

material: E=205,000 MPa, σ_y=300 MPa, α=11.7x10 $^{-6}$/°C
stiffener: t_w = 7.8 mm, h_w = 200 mm, t_f = 16.3 mm, b_f = 102 mm
(1) w_s=w_o=0.01l (2) w_s=w_o=0.005l (3) w_s=w_o=0.002l (4) w_s=w_o=0.0002l (5) w_s =0.0002l, w_o=0.1$\beta^2 t_p$
(6) w_s = 0.0002l, w_o = 0.1 β^2 t_p (β = 1,2 Temp = 200°C, β = 3, 4 Temp = 150°C)

Table 2
Summary of the Geometry and the Maximum Stress Ratio (σ/σ_y) of the Stiffened Plates

not enough finite element data points to construct design criteria at this stage. More analyses are necessary to establish a more complete database.

Acknowledgements

The technical support of Dr. Jan Walczak of ADINA R & D, Inc. is gratefully acknowledged.

References

1. "Design Standard DMEM 10, Structural Design of Surface Warships," Part I, II and III, Canadian Forces, 1978.

2. Naval Engineering Standard 110, Issue 2, Structures Manual Vol. 1 to 5, Ministry of Defense, Controllerate of the Navy, UK, 1985.

3. "Design of Surface Ship Structures," Vol. 1 and 2, Sea Systems Controllerate Publication No. 23 (SSCP23), Ministry of Defence, UK, 1989.

4. "Cold Formed Steel Structural Members CAN3-S136-M84," Standard Council of Canada, 1984.

5. "Preliminary Standard S473-M1989 Steel Structures," Canadian Standard Association, December, 1989.

6. "ADINA-IN for ADINA Users Manual," Report ARD 90-4, ADINA R & D, Inc., Sept. 1990.

7. Hu, S.Z., "An Analytical Investigation of the Compressive Behavior of Fabricated Steel Tubes," Ph.D. Dissertation, Dept. of Civil Engineering, University of Toronto, 1991.

8. Hu, S.Z., Birkemoe, P.C. and Prion, H.G.L., "Finite Element Modelling of Imperfections and Residual Stresses in Fabricated Tubular Columns," Design of Marine and Offshore Structures, Computational Mechanics Publications, 1992, pp.709-720.

9. Faulkner, D., "A Review of Effective Plating for Use in the Analysis of Stiffened Plating in Bending and Compression," J. of Ship Research, Vol. 19, No. 1, March 1975, pp 1-17.

10. Faulkner, D., Adamchak, J.C., Snyder, G.J. and Vetter, M.F., "Synthesis of Welded Grillages to Withstand Compression and Normal Loads," Computer and Structures, Vol. 3, 1973, pp. 221-246.

11. "Ship Structural Design Concepts," Ship Structure Committee, Edited by J.H. Evans, M.I.T., under Department of the Navy, Naval Ship Engineering Center, 1974.

12. "Guide to Stability Design Criteria for Metal Structures," Column Research Council, edited by Bruce G. Johnston, 1976.

13. Bleich, F., "Buckling Strength of Metal Structures," McGraw-Hill Book Company, 1952.

14. Winter, G., "Performance of Thin Steel Compression Flanges," Pub. 3rd Congr. Assoc. Bridge and Structural Eng., Liége, 1948.

15. Smith, C.S., Davidson, P.C., Chapman, J.C. and Dowling, P.J., "Strength and Stiffness of Ships' Plating under In-plane Compression and Tension," Trans. RINA, Vol. 130, 1988.

16. "Hand Book of Steel Construction CAN3-S16-M84," Canadian Institute of Steel Construction, 4th edition, 1985.

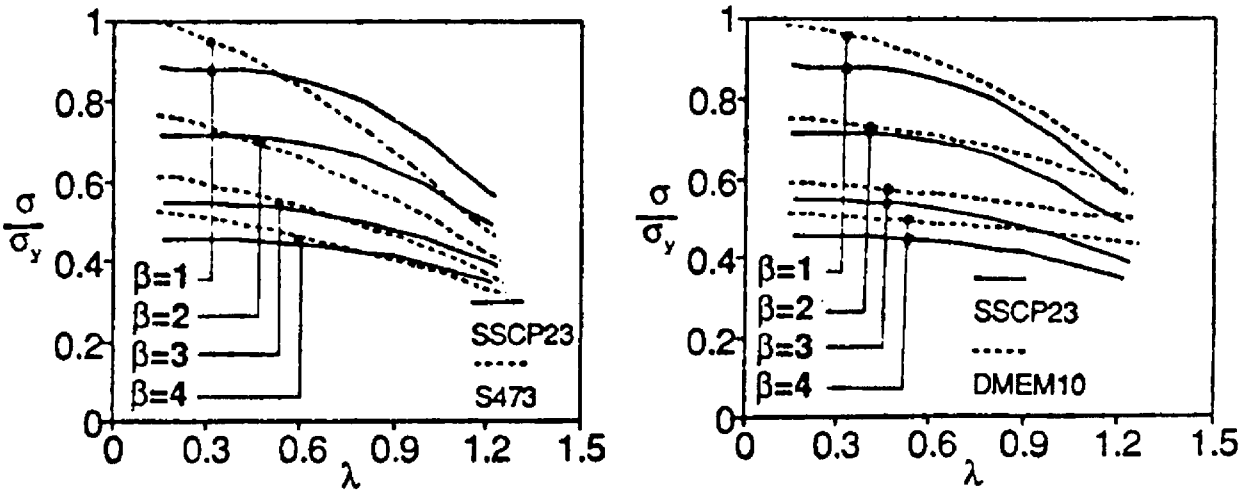

Figure 1
Comparison of Design Curves in Different Standards

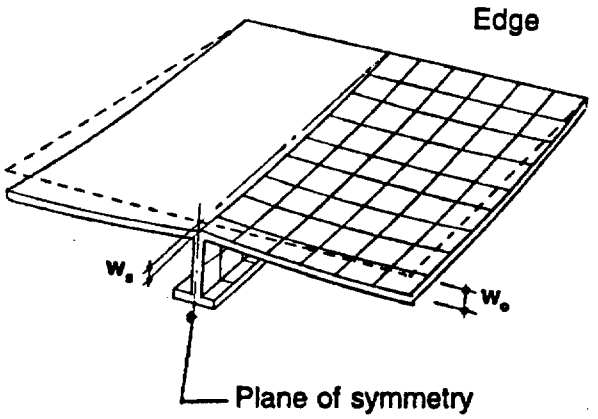

Figure 2
Imperfections in a Typical Stiffened Plate

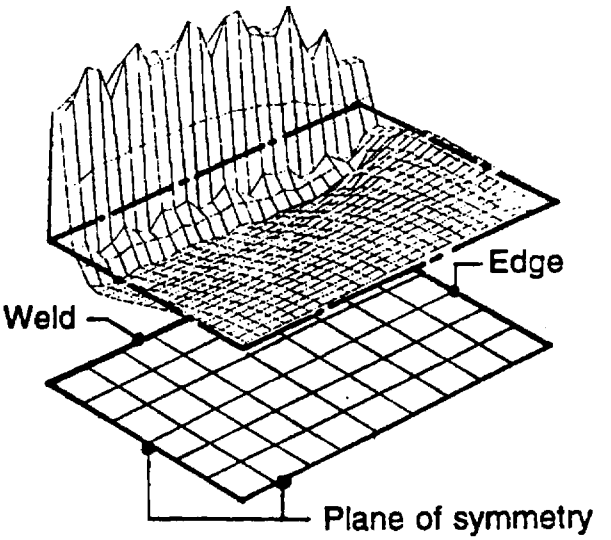

Figure 3
Possible Residual Stress Distribution in a Plate

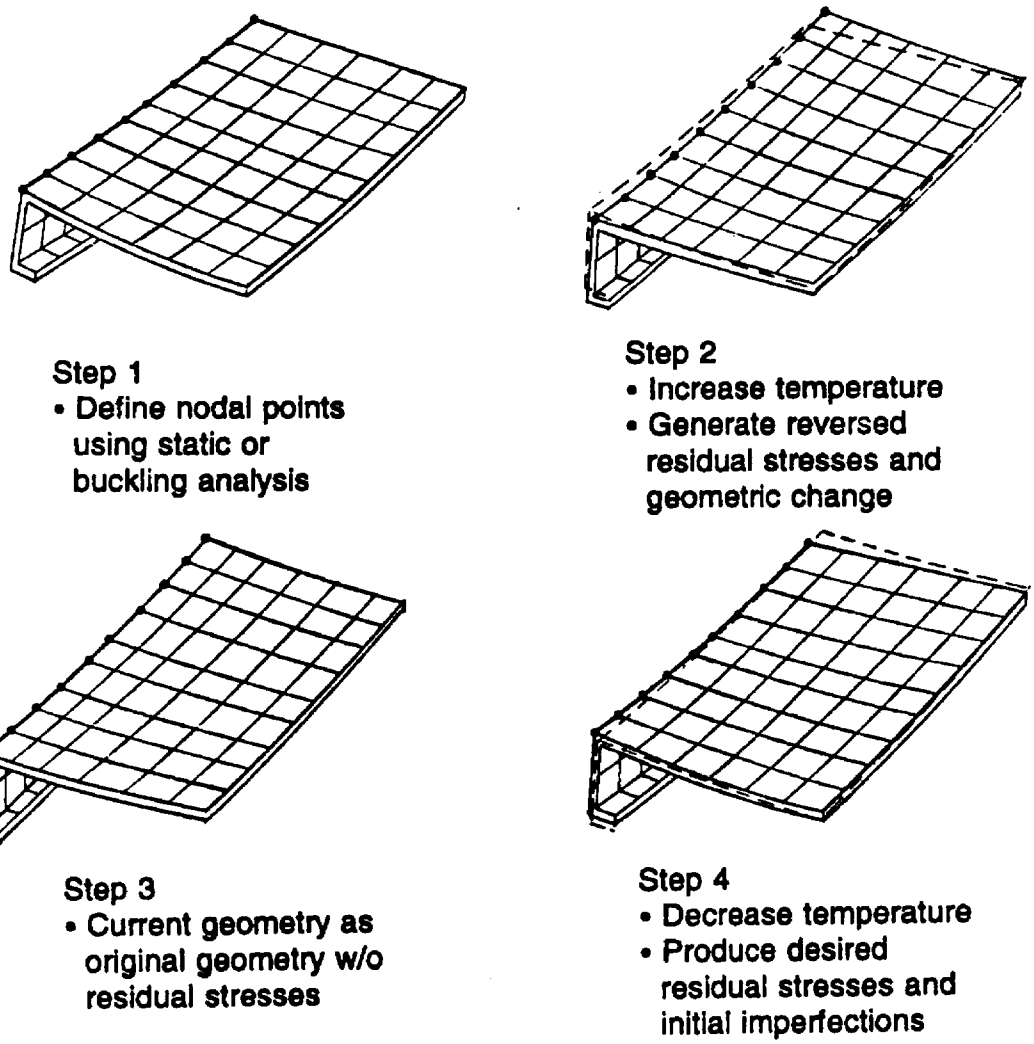

Figure 4
Procedure to Include Imperfections and Residual Stresses into Finite Element Model

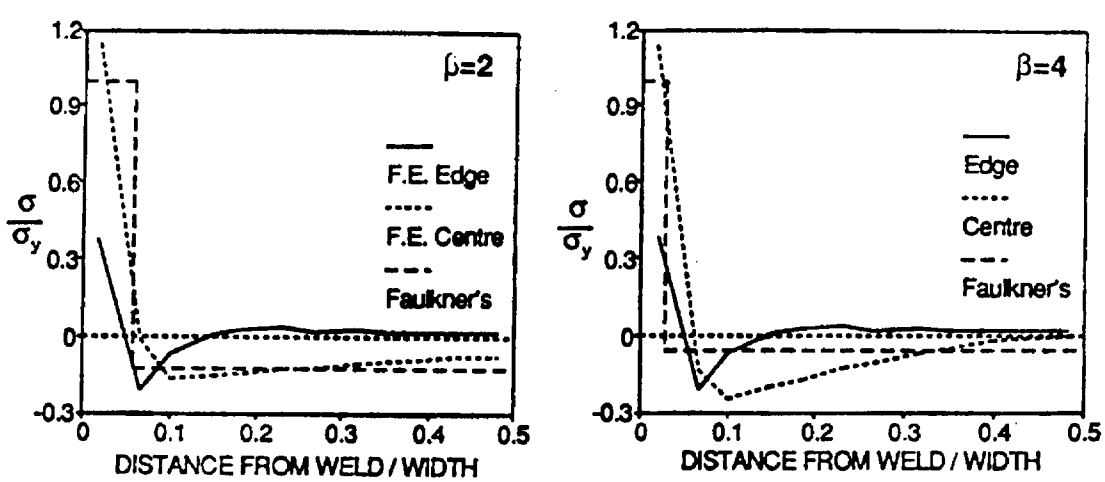

Figure 5
Comparison of Residual Stresses between Finite Element Results and Faulkner's Pattern

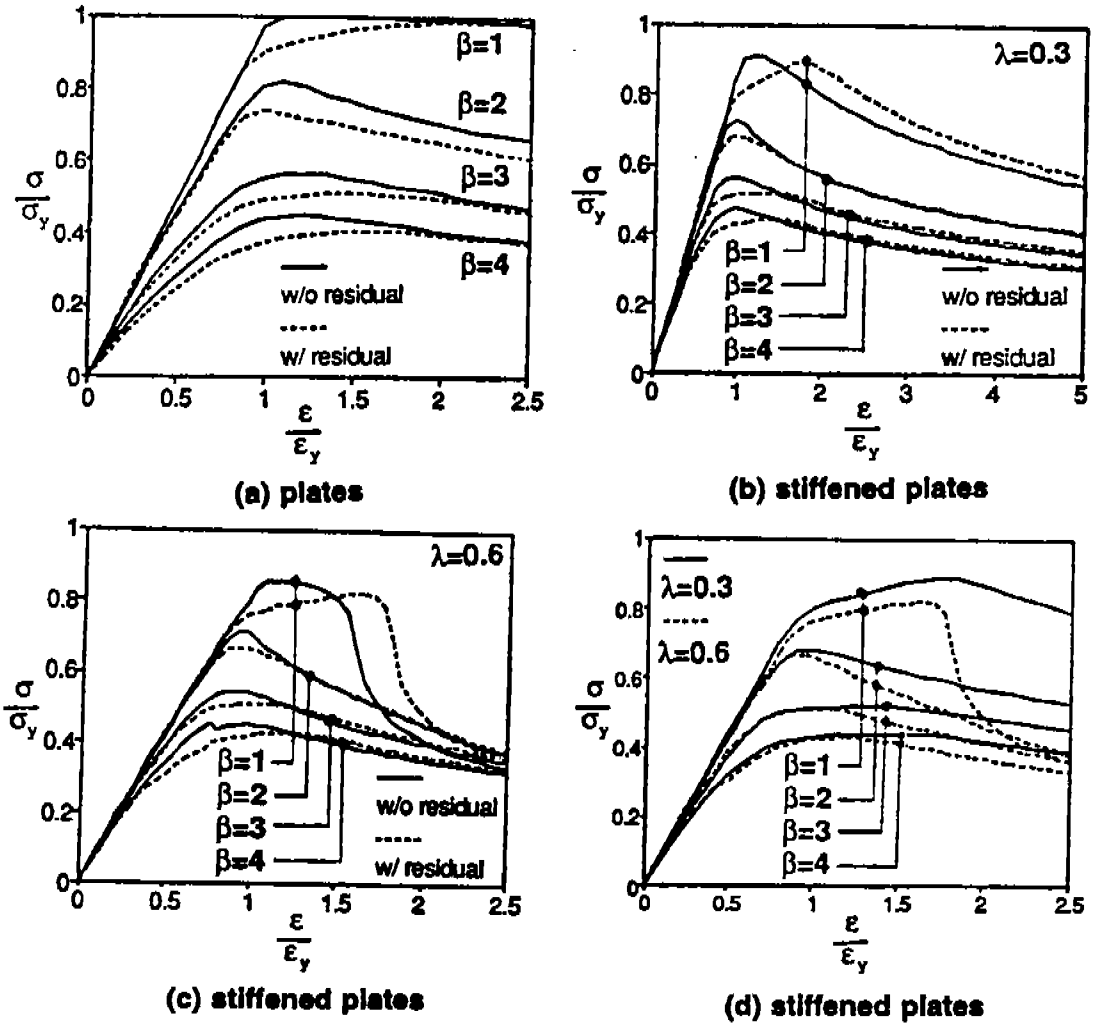

Figure 6
Comparison of Load-Displacement Curves of Plates and Stiffened Plates with Different Slenderness Ratios

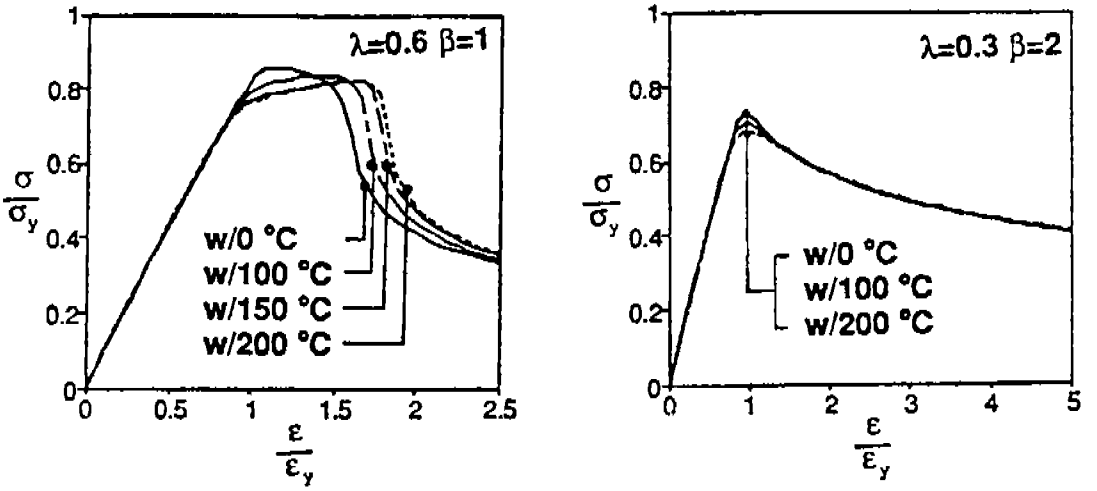

Figure 7
Comparison of Load-Displacement of Models with Different Residual Stress Level

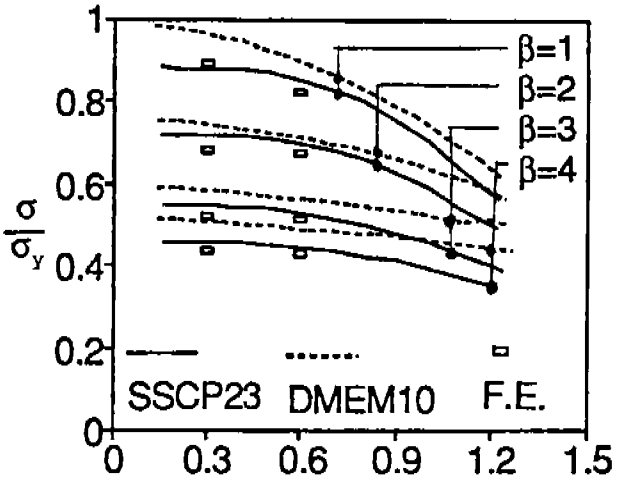

Figure 8
Comparison of Buckling Stress between Finite Element Results and Design Standards